

1 **The association between stratospheric weak polar vortex events and**
2 **cold air outbreaks**

3

4 Erik W. Kolstad & Tarjei Breiteig

5 Bjerknes Centre for Climate Research, Bergen, Norway

6 Adam A. Scaife

7 Hadley Centre for Climate Prediction and Research, Met Office, Exeter, United Kingdom

8

9 This paper was submitted to *Quarterly Journal of the Royal Meteorological Society* on 5 June
10 2009.

11

11
12
13
14
15
16
17
18
19
20
21
22
23
24
25
26
27
28
29
30
31

Abstract

Previous studies have identified an association between near-surface temperature anomalies in the Northern Hemisphere and weak stratospheric polar westerlies. Large regions in northern Asia, Europe and North America have been found to cool in the mature and late stages of stratospheric weak vortex events. A substantial part of the temperature changes are associated with changes to the tropospheric Northern Annular Mode and North Atlantic Oscillation pressure patterns. The apparent coupling between the stratosphere and the troposphere may be of relevance for weather forecasting, but only if the temporal and spatial nature of the coupling is known. Here we show, using 51 winters of re-analysis data, that the tropospheric temperature development relative to stratospheric weak polar vortex events goes through a series of well-defined stages, including geographically distinct cold air outbreaks. At the inception of weak vortex events, a precursor signal in the form of a strong high-pressure anomaly is found over Northwest Europe. At the same time, long-lived and robust cold anomalies appear over Asia and Western Europe. A few weeks later, near the mature stage of weak vortex events, a shorter-lived cold anomaly emerges off the east coast of North America. The probability of cold air outbreaks in different phases of the weak vortex life cycle increases by 50–80 % in four key regions. This shows that the stratospheric polar vortex contains information that can be used to enhance forecasts of cold air outbreaks. 300-year pre-industrial control runs of 11 state-of-the-art coupled climate models corroborate our results.

31

32 **1 Introduction**

33 Cold air outbreaks (CAOs) are departures of cold air masses into warmer regions. Over land,
34 these events can lead to excess deaths and damage to infrastructure. Over the ocean, marine
35 CAOs are important for a number of reasons: they give rise to mesoscale weather phenomena
36 such as polar lows (Bracegirdle and Gray, 2008), they lead to enhanced heat and momentum
37 fluxes from the ocean to the air (Renfrew and Moore, 1999) and may therefore influence the
38 ocean circulation (Pickart et al., 2003), and they cause rapid formation of sea ice in marginal ice
39 zones (Skogseth et al., 2004).

40 In recent years it has emerged that anomalies in the stratospheric circulation can be associated
41 with tropospheric CAOs (Thompson et al., 2002; Cai and Ren, 2007; Scaife et al., 2008).

42 Normally, the extra-tropical stratosphere is characterized by a strong westerly circumpolar flow.

43 In winter, planetary waves of tropospheric origin continuously propagate into the stratosphere
44 (Charney and Drazin, 1961), where they break and exert a drag on the zonal flow (McIntyre and
45 Palmer, 1983). This violates geostrophic balance and induces a poleward drift of air masses. At
46 high latitudes, the air converges, sinks and warms adiabatically. If there is more wave-breaking
47 than normal, the stratospheric zonal flow weakens and the polar stratosphere warms, giving rise
48 to Stratospheric Sudden Warmings (SSWs; Matsuno, 1971). These conditions may last for days
49 to weeks (Limpasuvan and Hartmann, 1999).

50 After their first appearance in the upper stratosphere, circulation anomalies are occasionally
51 found at successively lower levels (Matsuno, 1970; Lorenz and Hartmann, 2003). After reaching
52 the tropopause, the anomalies may impact the troposphere through an interaction with synoptic-

53 scale eddies, or more directly through induced meridional circulations (Song and Robinson,
54 2004). The result are negative Northern Annular Mode (NAM; Thompson and Wallace, 2001)
55 and North Atlantic Oscillation (NAO; Hurrell et al., 2003) patterns near the surface some weeks
56 after the first warming signal in the upper stratosphere.

57 Negative NAM and NAO regimes in the troposphere have a profound influence on the weather
58 in large and widespread regions of the Northern Hemisphere. Atlantic and Pacific storm tracks
59 shift latitudinally (Hurrell and Van Loon, 1997; Baldwin and Dunkerton, 2001), Greenland and
60 Newfoundland warms (Thompson et al., 2002), and the frequency and severity of CAOs increase
61 over large parts of East Asia (Jeong and Ho, 2005), northern Eurasia and the north-western part
62 of North America (Thompson and Wallace, 2001; Walsh et al., 2001; Cellitti et al., 2006). Over
63 the ocean, negative phases of the NAO, and positive height anomalies over Greenland in
64 particular, have been found to be associated with marine CAOs over the Nordic Seas (Kolstad et
65 al., 2008).

66 Motivated by the observed link between anomalous stratospheric events and the tropospheric
67 climate, we aim to provide a detailed description of tropospheric cold anomalies relative to such
68 events. Thompson et al. (2002) investigated the mean temperature response in the first 60 days
69 after the onset dates of stratospheric anomalous vortex conditions. Here we extend their work by
70 assessing the temperature development and changes to the probability of CAOs at different
71 stages of stratospheric weak vortex events. We do so for both continental and oceanic regions.
72 We find that the tropospheric temperature development goes through several distinct and well-
73 defined stages of stratospheric weak vortex events. CAOs over both continental and oceanic
74 regions are identified. These results are corroborated by data from 300-year time slices of 11
75 coupled model runs.

76

77 **2 Data and methods**

78 Daily mean fields from the NCEP/NCAR re-analysis (NNR) data (Kalnay et al., 1996) were used
79 throughout the study. The analysis period was from the autumn/winter of 1958 to the
80 winter/spring of 2009.

81 Monthly mean data from 11 models in the World Climate Research Programme's Coupled Model
82 Intercomparison Project phase 3 (CMIP3) multi-model dataset were also used. The models'
83 originating groups and countries, abbreviations, horizontal and vertical resolutions, highest
84 pressure levels and the model years that were used in this study are listed in Table I. For each
85 model, 300-year time slices of the «pre-industrial control run», with no anthropogenic or natural
86 forcing, were used. These were chosen arbitrarily from the years that were available for
87 download.

88 The most commonly used measure of stratospheric variability is the NAM index. However, as
89 both the spatial structure and the temporal variability of the NAM differed greatly across the
90 models, we used a Vortex Strength Index (VSI), defined below, as our indicator of stratospheric
91 variability. 50 hPa was the highest pressure level for which data from all the models was
92 available, so this was used as the stratospheric reference level for both the models and NNR.

93 The daily VSI was computed from NNR as follows. For each winter (December–February; DJF)
94 each day is defined by its date D and its year Y . $\Phi_{D,Y}$ is defined as the daily area-averaged
95 geopotential height at 50 hPa north of 65°N . From this time series, the date-wise climatological
96 mean μ_D^Φ and standard deviation σ_D^Φ were computed for 31-day windows surrounding the dates,

97 so that $\mu_D^\Phi = \sum_y \sum_{d=D-15}^{D+15} \Phi_{d,y}$ and $\sigma_D^\Phi = \sqrt{\sum_y \sum_{d=D-15}^{D+15} (\Phi_{d,y} - \mu_D^\Phi)^2}$. The daily, dimensionless VSI is given

98 by $-\left(\Phi_{D,Y} - \mu_D^\Phi\right) / \sigma_D^\Phi$. The minus sign is there because strong vortices are characterized by

99 negative height anomalies. The monthly VSI was computed from the model data in a similar
100 way, without the smoothing.

101 The analysis in this paper is centred on composites of days and months for which the
102 stratospheric vortex is weak. A *weak vortex day* in NNR is a day for which the daily VSI falls
103 below its overall 10th percentile. Similarly, a *weak vortex month* in the models is a month for
104 which the monthly VSI is less than its overall 10th percentile.

105 Weak vortex day number i in NNR is referred to as d_j^i , where i is an integer between 1 and N ,
106 the total number of such days. With 51 winters, each consisting of 90 days, N is 459. We define
107 an N -*composite* as an average over all the N cases. The N -composites of daily tropospheric
108 anomalies were computed as follows. If $Z'(d_j^i)$ is the i th geopotential height anomaly j days
109 *after* (if j is positive, or *before* if j is negative) the weak vortex days, the N -composite height
110 anomaly in the time interval from 0 to 20 days after the weak vortex days is

111 $\bar{Z}'_0^{20} \equiv \frac{1}{21 \times N} \sum_{i=1}^N \sum_{j=0}^{20} Z'(d_j^i)$. The same procedure is used for N -composite temperature anomalies

112 \bar{T}' .

113 The statistical significance of the N -composite anomalies was computed by means of Monte
114 Carlo experiments. Each d_j^i is defined at a specific date D and in a specific year Y . For
115 geopotential height, 500 artificial \hat{Z}'_k , for which the *years* of the d_j^i were permuted at random
116 from the analysis period, while the original *dates* were kept fixed, were constructed. With this

117 method, the seasonal cycle of the original N -composites is retained. Furthermore, to preserve the
 118 autocorrelation between the d_j^i , any d_j^i from the same year in the original N -composite were
 119 given the same year in the \hat{Z}'_k . An N -composite anomaly \bar{Z}' is considered significantly different
 120 from climatology (at the 0.05 level) if it was lower than the 0.025 quantile or greater than the
 121 0.975 quantile of the \hat{Z}'_k .

122 Four domains that illustrate the spatial extent of tropospheric cold anomalies are defined in Table
 123 II. For each of these domains, $T_{D,Y}$, area-averaged daily time series of 700-hPa temperature were
 124 computed. These time series were adjusted for seasonality and standardized in the same way as
 125 the VSI above, i.e. the temperature index is given by $(T_{D,Y} - \mu_D^T) / \sigma_D^T$. A *CAO day* is a day for
 126 which this index is lower than its overall 10th percentile.

127

127

128 **3 The Daily Vortex Strength Index**

129 In Figure 1(a), a matrix of VSI values for each day in the analysis period is shown. The blue days
130 are the d_0^i . Although the figure shows that weak vortex events can last for weeks, all the d_0^i are
131 considered as separate incidents in this study. An alternative would be to decide on a key date for
132 each event, e.g. the day that the VSI starts declining or the day that it hits its minimum. That
133 methodology was used by Charlton and Polvani (2007), and their central dates of SSWs are
134 shown with crosses in Figure 1(a). An advantage of such an approach is that all the events are
135 independent, and the study of lead/lag processes is free of effects of artificial smoothing.
136 However, a disadvantage is that one must be certain that the correct reference date has been
137 chosen in each case. Our approach is sensitive to only one a priori choice: the selection of a
138 threshold value for weak vortex days.

139 As our method leads to an artificial smoothing of the temporal signal, we average over rather
140 long time intervals and adopt the terminology of Limpasuvan et al. (2004). They examined the
141 evolution of wave activity fluxes and atmospheric pressure fields in several sub-periods of SSW
142 life cycles, and defined the following phases of weak vortex events: *onset* (60–41 days before the
143 d_0^i), *growth* (40–21 days before the d_0^i), *early mature* (20–1 days before the d_0^i), *late mature* (0–
144 20 days after the d_0^i), *decline* (21–40 days after the d_0^i) and *decay* (41–60 days after the d_0^i).
145 Note that the developments in Figure 9 in Limpasuvan et al. (2004) are not necessarily directly
146 comparable to the developments in our time intervals.

147 In Figure 1(b), the N -composite average of the VSI index is shown with up to 60 days of
148 lag/lead-time relative to the d_0^i . The slopes of the curve on either side of day zero are indicators
149 of the autocorrelation of the VSI near weak vortex events.

150

150

151 **4 Results**

152 4.1 Composite analysis of daily data

153 In this section, N -composites of daily 500-hPa geopotential height and temperature (from NNR)
154 anomalies relative to the d_0^i are analyzed. The temporal development in the troposphere
155 throughout the life cycle of stratospheric weak vortex events is presented with an emphasis on
156 cold anomalies. Figure 2 shows the development of 500-hPa geopotential height anomalies
157 averaged over the weak vortex stages specified in Section 3. Figure 2 provides the dynamical
158 framework to interpret the 700-hPa potential temperature anomalies in Figure 3.

159 In the *onset* phase (Figure 2(a)), a positive anomaly centred over northern Scandinavia (H0 in
160 Figure 2) and a negative anomaly near the Bering Strait are found. This corresponds to a pattern
161 found to favour stratospheric warmings through upward-propagating tropospheric waves
162 (Kuroda and Kodera, 1999; Breiteig, 2009; Garfinkel et al., 2009) and is a tropospheric precursor
163 of the warming aloft.

164 H0 is present throughout all the stages and moves westwards with time. In Figure 2(a), two
165 additional negative height anomalies are found, one over Northeast Asia (L1) and another over
166 the western Mediterranean (L2). These two anomalies constitute a wave together with H0. L1
167 and L2 persist for all the stages without migrating substantially. A third negative height anomaly
168 (L3) emerges to the south of Newfoundland in Figure 2(b).

169 In Figure 3, three distinct and persistent cold anomalies are found: C1 over Northeast Asia is
170 associated with L1; C2 at different locations over Europe and the Nordic Seas is associated with
171 L2; and C3 off the coast of North America is associated with L3.

172 In addition, there is an early cold anomaly in the western part of the Bering Sea and the Sea of
173 Okhotsk in the *growth* phase (Figure 3(b)) that is associated with the Bering Sea negative height
174 anomaly.

175

176 4.2 Model ensemble analysis

177 We now examine monthly mean data from the 11 coupled climate models in Table I. Figure 4
178 shows the 700-hPa temperatures during weak vortex months (b), as well as in the preceding (a)
179 and succeeding (c) months. For comparison, parts of the temperature development from the re-
180 analysis (Figure 3) are shown again, but now with averaging periods corresponding to the ones
181 for the models.

182 The following features are present in both the model results for the months before weak vortex
183 months (Figure 4(a)) and in NNR 16–45 days prior to the d_0^i (Figure 4(d)): a cold anomaly over
184 the Bering Sea and the Sea of Okhotsk, C1 over Asia, C2 over Europe, and warm anomalies over
185 the Nordic Seas region and northern North America.

186 The westward shift of the Nordic Seas warm anomaly, the northward spread of C2, and the
187 appearance of C3 off the coast of North America in the month surrounding the d_0^i (Figure 4(e))
188 are all seen in the model ensemble during weak vortex months (Figure 4(b)). The pattern formed
189 by these anomalies, along with the warm anomaly near the Caspian Sea, is reminiscent of the
190 typical NAO quadrupole temperature pattern (Stephenson and Pavan, 2003). In the same time
191 period, C1 is more zonally elongated in the models than in NNR, covering parts of the Northwest
192 Pacific, and C3 covers more of North America.

193 In the late stages of weak vortex event life cycles, C2, now centred over Scandinavia in NNR
194 (Figure 4(f)), is present in the models (Figure 4(c)). C1 over Asia is weaker in the models than in
195 NNR at this stage.

196 In summary, the most pronounced cold anomalies in Figure 3 are well matched by cold
197 anomalies in an ensemble of 11 coupled climate models.

198

199 4.3 Regional cold anomalies

200 In this section, we use time series of area-averaged and standardized 700-hPa temperature
201 anomalies to assess whether or not information about the state of the stratospheric polar vortex
202 has an impact on the forecasting of CAOs in the four regions in Table II.

203 CAO days were defined above as the days with temperatures lower than the overall 10th
204 percentile. We now define the ratio r as the total number of CAO days in each stage of a weak
205 vortex event divided by the climatological mean number of CAO days on the same dates of the
206 year throughout the analysis period. When $r > 1$ for a specific stage, CAOs are more likely than
207 normal during that stage of weak vortex events.

208 In Figure 5, N -composites of (non-standardized) temperature anomalies relative to the d_0^i (a) and
209 the ratio r (b) are shown for each region and for the different stages of weak vortex events.

210 In the NEA domain (green curves in Figure 5), the East Asia winter monsoon ridge-trough
211 pattern (Compo et al., 1999) in Figure 2 maintains a steady flow of cold air into the region and
212 lower-than-normal temperatures are found throughout the life cycle of weak vortex events
213 (Figure 5(a)). In the *growth*, *early mature* and *decay* stages, CAOs occur about 70–80 % more

214 often than normal (Figure 5(b)), with temperatures between 1 K and 1.4 K lower than normal.

215 The *decline* phase sees about 50 % more CAOs and temperatures 0.9 K lower than normal.

216 In the EUR domain (red curves in Figure 5), CAOs are about 50 % (40 %) more likely than

217 normal in the *growth (decline)* phase, with temperatures about 0.7 K lower than normal. This is

218 consistent with C2 covering large parts of this region in Figure 3(b) and 3(e).

219 As C2 moves northward into the NS domain in the *late mature* phase (Figure 3(d)), L2 expands

220 towards the north (Figure 2(d)), and H0 weakens the climatological trough west of Iceland. An

221 anomalous ridge-trough pattern emerges between Greenland and Central Europe, and the flow

222 field veers towards the north. The interplay between an anomalous ridge over Greenland/Iceland

223 and an anomalous trough over Scandinavia was found by Kolstad et al. (2008) to be associated

224 with marine CAOs over the Nordic Seas. Indeed, CAOs are about 60 % more likely than normal

225 and temperatures are about 1 K lower than normal in the *late mature* and *decline* phases (black

226 curves in Figure 5).

227 In WNA (blue curves in Figure 5), the lowest temperatures are found in the *mature* phase.

228 Around this time the development of L3 and the ridging in the Baffin Island region (Figure 2(c)–

229 (d)) are symptoms of a southward displacement of the 500-hPa «polar vortex» in Cellitti et al.

230 (2006). This situation is associated with substantial cold air advection and C3 in Figures 3(c)–

231 (d). The chance of CAOs in the region increase by about 40 % in the *early mature* phase and

232 about 60 % in the *late mature* phase of stratospheric weak vortex events. Temperatures are 0.6 K

233 and 1 K lower than normal, respectively.

234

234

235 **5 Concluding remarks**

236 The relationship between stratospheric weak vortex events and tropospheric developments, and
237 cold air outbreaks (CAOs) in particular, were investigated by using 51 winters of re-analysis
238 data. The life cycle of a weak vortex event was separated into six 20-day periods (following
239 Limpasuvan et al., 2004): the *onset*, *growth*, *early mature*, *late mature*, *decline* and *decay* phases.

240 The clearest precursor of stratospheric weak vortex events was found to be a high pressure
241 anomaly centred over northern Scandinavia in the *onset* and *growth* phases. This positive height
242 anomaly persisted for all the phases and was contained to the high latitudes in the Atlantic sector.

243 A major motivation for studying the troposphere-stratosphere interactions is the prospect of
244 prediction. A ratio r was defined as the total number of CAO days in each stage of a weak vortex
245 event divided by the climatological mean number of CAO days on the corresponding dates. The
246 probability of CAOs was found to increase:

- 247 • by about 70–80 % in the *growth*, *early mature* and *decay* phases and by about 50 % in
248 the *decline* phase in Northeast Asia.
- 249 • by about 50 % in the *growth* phase and by about 40 % in the *decline* phase in Central
250 Europe.
- 251 • by about 60 % in the *late mature* and *decline* phases in northern Scandinavia, including
252 the Nordic Seas.
- 253 • by about 40 % in the *early mature* phase and by about 60 % in the *late mature* phase off
254 the east coast of North America.

255 Parts of the analysis were repeated with an ensemble of 11 coupled climate models. Somewhat
256 surprisingly, considering that many of these models do not have a well-resolved stratosphere, the
257 model results corroborated the relationships between weak vortex events and the cold anomalies
258 listed above. This may indicate that the main aspects of the tropospheric temperature
259 development during the life cycle of stratospheric weak vortex events are associated with
260 internal processes in the troposphere and lower stratosphere.

261

261 **Acknowledgements**

262 Erik Kolstad's work was funded by the Norwegian Research Council through its International
263 Polar Year programme and the project IPY-THORPEX (grant number 175992/S30). Adam
264 Scaife was supported by the Joint DECC, Defra and MoD Integrated Climate Programme -
265 DECC/Defra (GA01101), MoD (CBC/2B/0417_Annex C5). This is publication no. X from the
266 Bjerknes Centre for Climate Research.

267

267

268

References

269

- 270 Baldwin MP, Dunkerton TJ. 2001. Stratospheric harbingers of anomalous weather regimes. *Science*. **294**: 581-584.
- 271 Bracegirdle TJ, Gray SL. 2008. An objective climatology of the dynamical forcing of polar lows in the Nordic seas.
272 *Int. J. Climatol.* **28**: 1903-1919.
- 273 Breiteig T. 2009. Tropospheric Precursors of Stratospheric Warmings. *Clim. Dyn.*: submitted.
- 274 Cai M, Ren RC. 2007. Meridional and downward propagation of atmospheric circulation anomalies. Part I:
275 Northern Hemisphere cold season variability. *J. Atmos. Sci.* **64**: 1880-1901.
- 276 Cellitti MP, Walsh JE, Rauber RM, Portis DH. 2006. Extreme cold air outbreaks over the United States, the polar
277 vortex, and the large-scale circulation. *J. Geophys. Res.* **111**: D02114.
- 278 Charlton AJ, Polvani LM. 2007. A new look at stratospheric sudden warmings. Part I: Climatology and modeling
279 benchmarks. *J. Climate*. **20**: 449-469.
- 280 Charney JG, Drazin PG. 1961. Propagation of planetary-scale disturbances from the lower into the upper
281 atmosphere. *J. Geophys. Res.* **66**: 83-109.
- 282 Compo GP, Kiladis GN, Peter J. Webster. 1999. The horizontal and vertical structure of east Asian winter
283 monsoon pressure surges. *Q. J. R. Meteorol. Soc.* **125**: 29-54.
- 284 Garfinkel CI, Hartmann DL, Sassi F. 2009. Tropospheric Precursors of Anomalous Northern Hemisphere
285 Stratospheric Polar Vortices. *J. Climate*. **submitted**.
- 286 Hurrell JW, Van Loon H. 1997. Decadal variations in climate associated with the North Atlantic Oscillation.
287 *Climatic Change*. **36**: 301-326.
- 288 Hurrell JW, Kushnir Y, Ottersen G, Visbeck M, 2003: An Overview of the North Atlantic Oscillation. *The North
289 Atlantic Oscillation: Climatic Significance and Environmental Impact*, J. W. Hurrell, Y. Kushnir, G. Ottersen, and
290 M. Visbeck, Eds., American Geophysical Union, 1--35.
- 291 Jeong J-H, Ho C-H. 2005. Changes in occurrence of cold surges over east Asia in association with Arctic
292 Oscillation. *Geophys. Res. Lett.* **32**.
- 293 Kalnay E, and Coauthors. 1996. The NCEP/NCAR 40-year reanalysis project. *Bull. Am. Meteorol. Soc.* **77**: 437-471.
- 294 Kolstad EW, Bracegirdle TJ, Seierstad IA. 2008. Marine cold-air outbreaks in the North Atlantic: temporal
295 distribution and associations with large-scale atmospheric circulation. *Clim. Dyn.* **published online in June**.
- 296 Kuroda Y, Kodera K. 1999. Role of Planetary Waves in the Stratosphere-Troposphere Coupled Variability in the
297 Northern Hemisphere Winter. *Geophys. Res. Lett.* **26**: 2375-2378.
- 298 Limpasuvan V, Hartmann DL. 1999. Eddies and the Annular Modes of Climate Variability. *Geophys. Res. Lett.* **26**:
299 3133-3136.
- 300 Limpasuvan V, Thompson DWJ, Hartmann DL. 2004. The life cycle of the Northern Hemisphere sudden
301 stratospheric warmings. *J. Climate*. **17**: 2584-2596.
- 302 Lorenz DJ, Hartmann DL. 2003. Eddy-zonal flow feedback in the Northern Hemisphere winter. *J. Climate*. **16**:
303 1212-1227.
- 304 Matsuno T. 1970. Vertical Propagation of Stationary Planetary Waves in the Winter Northern Hemisphere. *J. Atmos.
305 Sci.* **27**: 871-883.
- 306 Matsuno T. 1971. A Dynamical Model of the Stratospheric Sudden Warming. *J. Atmos. Sci.* **28**: 1479-1494.

- 307 McIntyre ME, Palmer TN. 1983. Breaking planetary waves in the stratosphere. *Nature*. **305**: 593-600.
- 308 Pickart RS, Spall MA, Ribergaard MH, Moore GWK, Milliff RF. 2003. Deep convection in the Irminger Sea
309 forced by the Greenland tip jet. *Nature*. **424**: 152-156.
- 310 Renfrew IA, Moore GWK. 1999. An extreme cold-air outbreak over the Labrador Sea: Roll vortices and air-sea
311 interaction. *Mon. Wea. Rev.* **127**: 2379--2394.
- 312 Scaife AA, Folland CK, Alexander LV, Moberg A, Knight JR. 2008. European climate extremes and the North
313 Atlantic Oscillation. *J. Climate*. **21**: 72-83.
- 314 Skogseth R, Haugan PM, Haarpaintner J. 2004. Ice and brine production in Storfjorden from four winters of
315 satellite and in situ observations and modeling. *J. Geophys. Res.* **109**: C10008.
- 316 Song Y, Robinson WA. 2004. Dynamical Mechanisms for Stratospheric Influences on the Troposphere. *J. Atmos.*
317 *Sci.* **61**: 1711-1725.
- 318 Stephenson DB, Pavan V. 2003. The North Atlantic Oscillation in coupled climate models: a CMIP1 evaluation.
319 *Clim. Dyn.* **20**: 381-399.
- 320 Thompson DWJ, Wallace JM. 2001. Regional climate impacts of the Northern Hemisphere annular mode. *Science*.
321 **293**: 85-89.
- 322 Thompson DWJ, Baldwin MP, Wallace JM. 2002. Stratospheric connection to Northern Hemisphere wintertime
323 weather: Implications for prediction. *J. Climate*. **15**: 1421-1428.
- 324 Walsh JE, Phillips AS, Portis DH, Chapman WL. 2001. Extreme cold outbreaks in the United States and Europe,
325 1948-99. *J. Climate*. **14**: 2642-2658.
- 326
- 327

Originating group(s)	Country	IPCC model designation	Horizontal resolution north of 20N	Number of vertical layers	Number of layers over 200 hPa	Top level	St. dev. of DJF 50-hPa geop. height (m)	Model years used
Bjerknes Centre for Climate Research	Norway	BCCR-BCM2.0	25x128	31	20	0.01 hPa	102	2370–2669
National Center for Atmospheric Research	USA	CCSM3	50x256	26	13	2.2 hPa	208	480–779
Canadian Centre for Climate Modelling & Analysis	Canada	CGCM3.1(T63)	25x128	31	N/A	N/A	179	1850–2149
Météo-France / Centre National de Recherches Météorologiques	France	CNRM-CM3	25x128	45	23	0.05 hPa	148	2130–2429
Max Planck Institute for Meteorology	Germany	ECHAM5/MPI-OM	37x192	31	9	10 hPa	118	2250–2549
US Dept. of Commerce / NOAA / Geophysical Fluid Dynamics Laboratory	USA	GFDL-CM2.1	35x144	24	5	3 hPa	153	199–498
Institut Pierre Simon Laplace	France	IPSL-CM4	28x96	19	8	N/A	184	2060–2359
Center for Climate System Research / National Institute for Environmental Studies / Frontier Research Center for Global Change	Japan	MIROC3.2(medres)	25x128	20	8	30 km	96	2500–2799
Meteorological Research Institute	Japan	MRI-CGCM2.3.2	25x128	30	16	0.4 hPa	190	1901–2200
National Center for Atmospheric Research	USA	PCM	25x128	26	13	2.2 hPa	170	150–449
Hadley Centre for Climate Prediction and Research / Met Office	United Kingdom	UKMO-HadCM3	29x96	19	N/A	N/A	151	1900–2199

Table I. The coupled climate models used in this study. More information and relevant references for each model can be found at <http://www-pcmdi.llnl.gov/>.

Region name	Abbreviated region name	Longitude range	Latitude range
Nordic Seas	NS	10°W–60°E	62.5°N–80°N
Central Europe	EUR	10°W–30°E	40°N–57.5°N
Western North Atlantic	WNA	90°W–40°W	30°N–47.5°N
Northeast Asia	NEA	80°E–140°E	42.5°N–65°N

Table II. The domains used in this study.

Figure Captions

Figure 1. (a) The standardized daily VSI, sorted and binned by quantiles. The SSW central dates in Charlton and Polvani (2007) are marked with crosses. (b) The N -composite standardized daily VSI (in quantile terms) for each day relative to weak vortex days.

Figure 2. N -composites of 500-hPa geopotential height anomalies (in m) relative to weak vortex days, averaged over the specified phases. Anomalies that are significant at the 0.05-level, according to a 500-member Monte Carlo experiment (see text for details), are marked with dots. Black contours are drawn along the values corresponding to the tick marks of the colour bar.

Figure 3. As Figure 2, but for 700-hPa temperature anomalies (in K). The boundaries of the four regions in Table II are drawn with black boxes.

Figure 4. (a–c): The model ensemble 700-hPa temperature anomalies (in K) relative to weak vortex months. (d–f) As Figure 3, but in the specified time intervals relative to weak vortex days.

Figure 5. For the four regions in Table II, the N -composite (a) area-averaged, non-standardized 700-hPa temperature anomalies relative to weak vortex days; and (b) number of CAO days divided by the climatological number of CAO days (the ratio r).

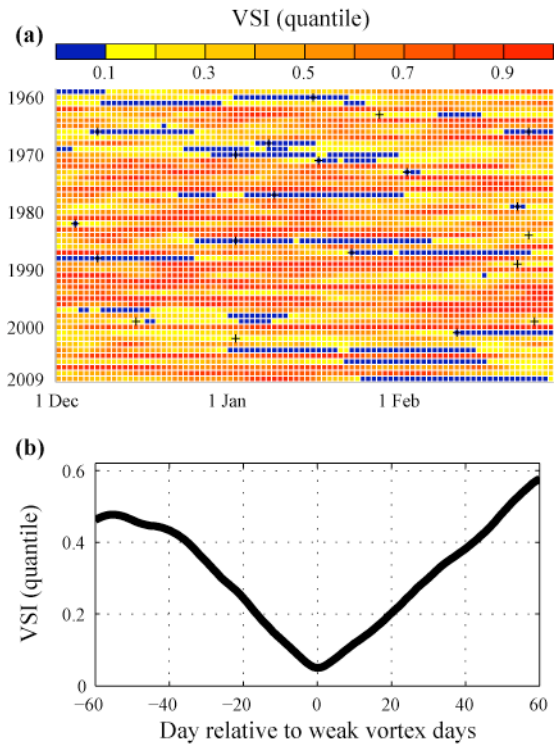


Figure 1. (a) The standardized daily VSI, sorted and binned by quantiles. The SSW central dates in Charlton and Polvani (2007) are marked with crosses. (b) The N -composite standardized daily VSI (in quantile terms) for each day relative to weak vortex days.

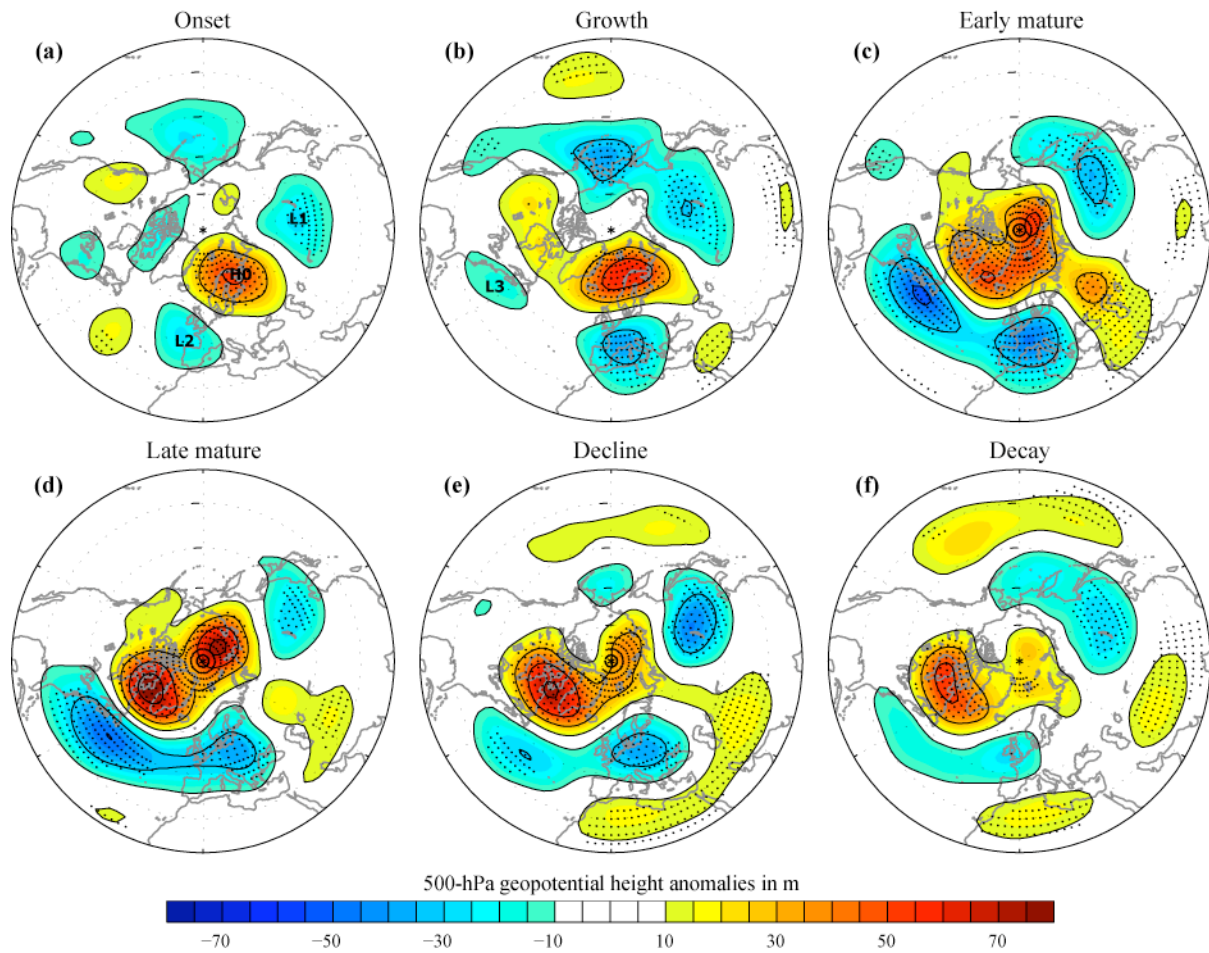


Figure 2. *N*-composites of 500-hPa geopotential height anomalies (in m) relative to weak vortex days, averaged over the specified phases. Anomalies that are significant at the 0.05-level, according to a 500-member Monte Carlo experiment (see text for details), are marked with dots. Black contours are drawn along the values corresponding to the tick marks of the colour bar.

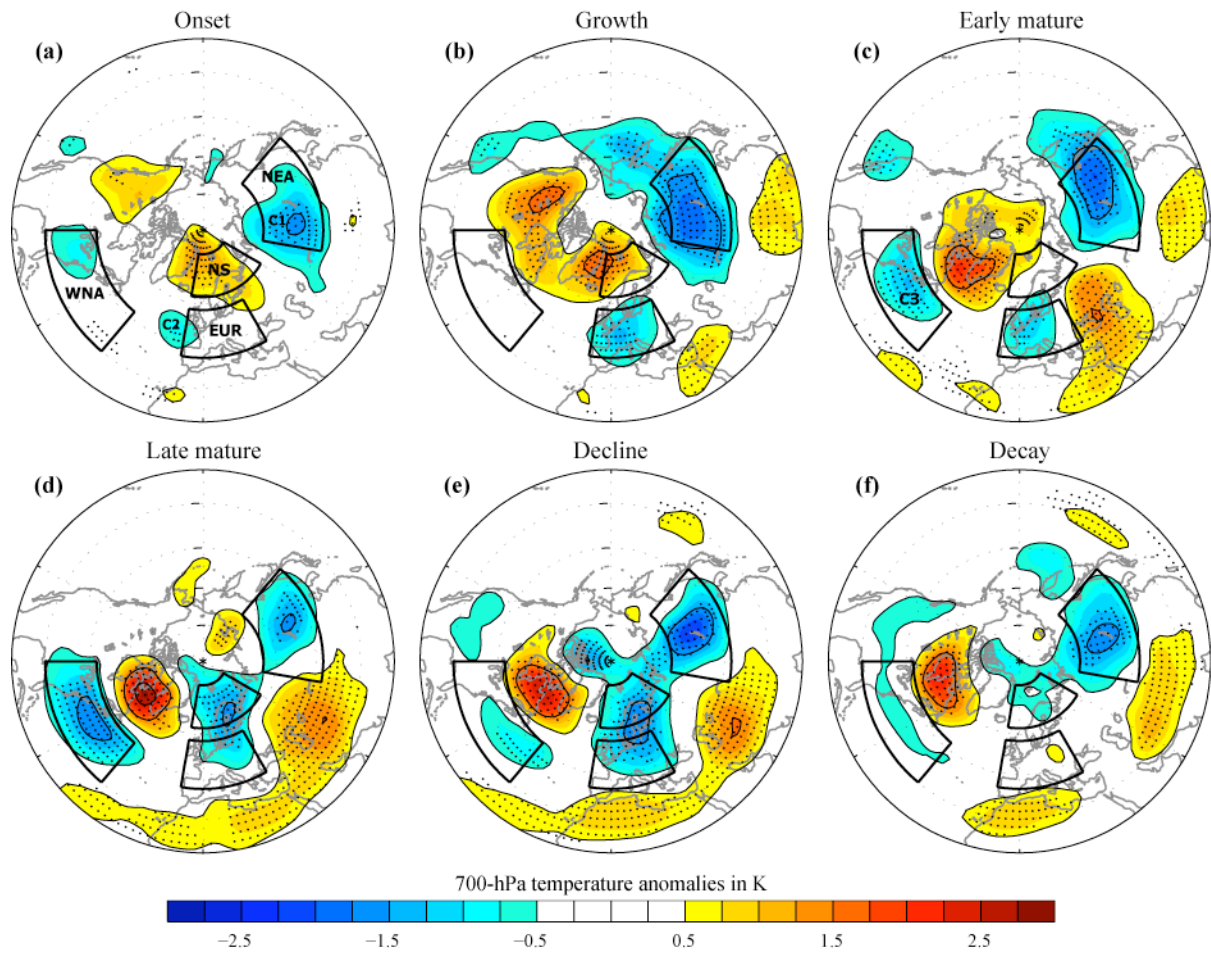


Figure 3. As Figure 2, but for 700-hPa temperature anomalies (in K). The boundaries of the four regions in Table II are drawn with black boxes.

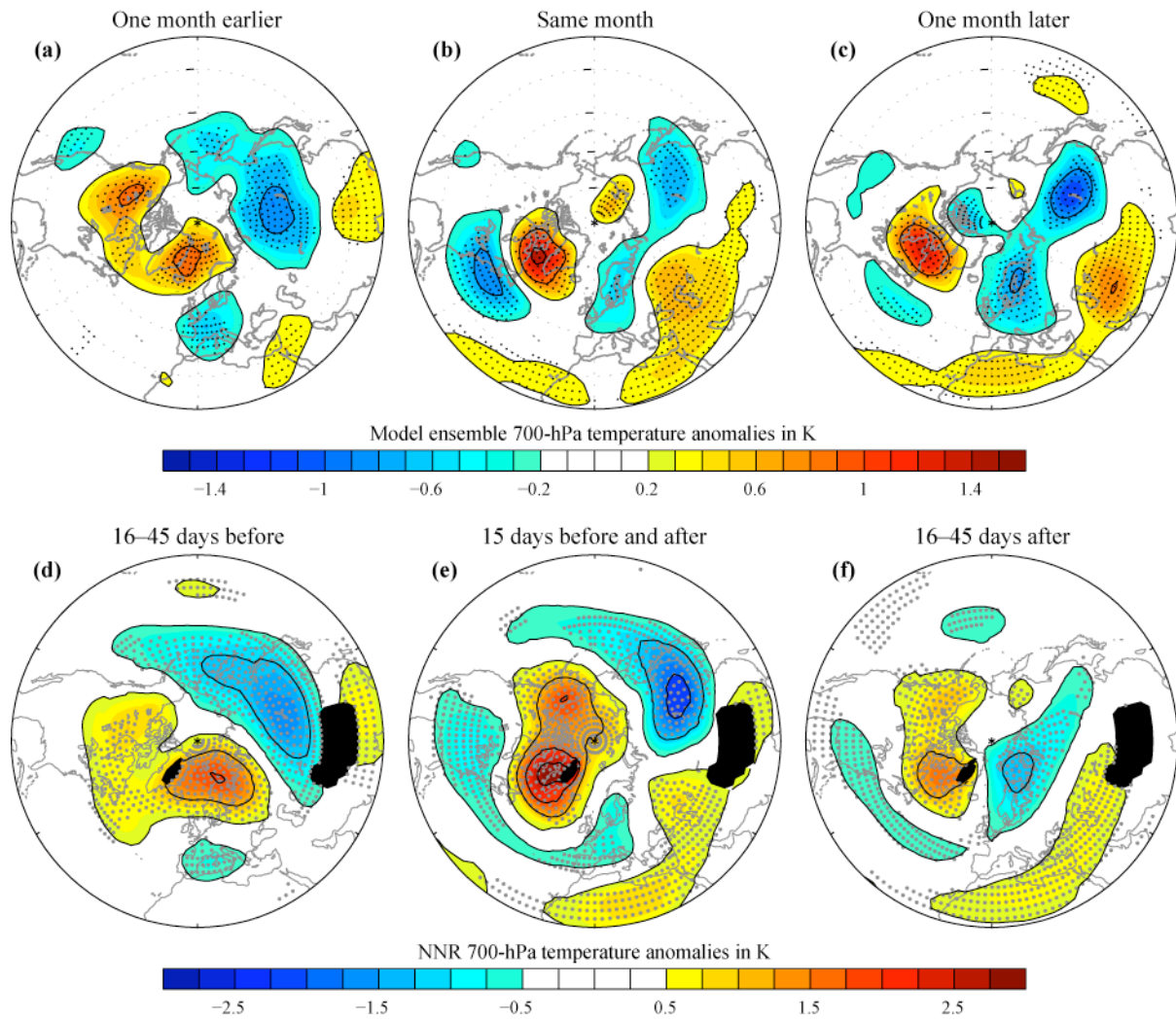


Figure 4. (a–c): The model ensemble 700-hPa temperature anomalies (in K) relative to weak vortex months. (d–f) As Figure 3, but in the specified time intervals relative to weak vortex days.

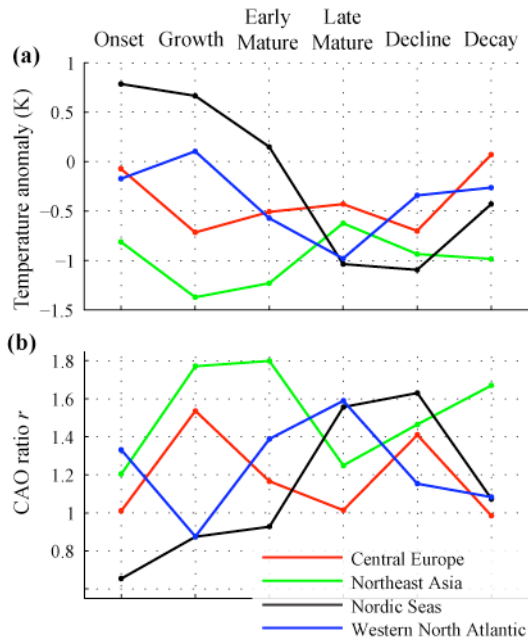


Figure 5. For the four regions in Table II, the N -composite (a) area-averaged, non-standardized 700-hPa temperature anomalies relative to weak vortex days; and (b) number of CAO days divided by the climatological number of CAO days (the ratio r).